Depth-resolved analysis of the effect of RbF post deposition treatment on CIGSe with two different Cu concentrations

Natalia Maticiuc[1,], Tim Kodalle[1,*], Bünyamin Ümsür[2], Tobias Bertram[1], Robert Wenisch[1], Yajie Wang[1], Isheta Majumdar[1], Hasan A. Yetkin[1,3], Daniel Abou-Ras[4], Norbert Schäfer[4], Christian A. Kaufmann[1], Rutger Schlatmann[1,5], Iver Lauermann[1]*

[1]Competence Centre Photovoltaics Berlin (PVcomB) / Helmholtz Zentrum Berlin für Materialien und Energie (HZB), Schwarzschildstr. 3, 12489 Berlin, Germany

[2]Department of Physics and BILTEM, Yozgat Bozok University, Atatürk Yolu 7. Km, 66900 Yozgat, Turkey

[3]Technology for Thin-Film Devices, Technische Universität Berlin, Einsteinufer Str. 25, 10587 Berlin, Germany

[4]Department Structure and Dynamics of Energy Materials (EM-ASD) / Helmholtz Zentrum Berlin für Materialien und Energie (HZB), Hahn-Meitner-Platz 1, 14109 Berlin, Germany

[5]Hochschule für Technik und Wirtschaft Berlin, Wilhelminenhofstr. 75a, 12459 Berlin, Germany

*Corresponding authors:

natalia.maticiuc@helmholtz-berlin.de (Dr. Natalia Maticiuc)

tim.kodalle@helmholtz-berlin.de (Dr. Tim Kodalle)

Tel: +49 30 8062 15698, Fax: +49 30 8062 15677

ABSTRACT

Photovoltaic devices based on Cu(In,Ga)Se_2 (CIGSe) absorbers are among the most attractive non-Si alternatives. The key to their steadily increasing efficiency is a post-deposition treatment (PDT) with alkali salts. For co-evaporated CIGSe, a RbF-PDT was demonstrated as the most efficient, however, the mechanism of the RbF influence on the CIGSe absorber is not completely understood. Here, we focus on the impact of RbF on the surface of co-evaporated CIGSe absorbers

in dependence on their bulk composition. Surface- as well as bulk- sensitive methods with overlapping information depths are used to examine an overall depth profile of RbF-free and RbF-treated CIGSe samples with different Cu contents. We show a gradual depletion of copper towards the surface for the as-deposited CIGSe absorber layers. The following RbF-PDT sharpens this effect especially for the sample grown with the overall lower Cu content. Under the Cu-depleted surface layer, the composition of the CIGSe gradually changes until it reaches the respective bulk composition. As a result of the RbF-PDT, Ga diffuses towards the surface and Rb gets incorporated at the surface where GaF_3 and $RbInSe_2$ secondary phases are formed, respectively. A higher Cu content leads to less surface oriented Ga diffusion, less Rb incorporation and to a thinner $RbInSe_2$ layer. A thinner $RbInSe_2$ barrier layer, in turn, maintains the gain in open-circuit voltage and prevents the fill factor loss of the CIGSe device.

KEYWORDS

$Cu(InGa)Se_2$; Hard X-ray Photoelectron Spectroscopy; Glow Discharge Optical Emission Spectroscopy, Alkali Treatment; Rubidium Fluoride.

1. INTRODUCTION

With the increasing demand for renewable energy, photovoltaic devices based on thin films have recently gained more interest. $Cu(In,Ga)Se_2$ (CIGSe) is one of the most attractive non-Si alternatives due to its steadily increasing efficiency. As with other alternative thin-film solar cells such as CdTe or SnS [1,2], a post-deposition treatment (PDT) has been proved as a key solution for CIGSe on its way to high performance More precisely, the efficiency of CIGSe solar cells was increased by 3% absolute since 2011 by complementing the traditionally used Na-doping [3] with the incorporation of a second alkali metal from K [4], to Rb [5], and finally to Cs [6] using such a PDT. The current record efficiency of 23.35% was reached using $Cu(In,Ga)(S,Se)_2$ deposited in a sequential process and subjected to a CsF-PDT [6]. For co-evaporated CIGSe absorbers however, the best performance of 22.6 % was obtained employing a RbF-PDT [5]. At Helmholtz Zentrum Berlin, with a similar co-evaporation approach, CIGSe solar cells with an (in-house) maximum efficiency of close to 21% were obtained [7].

The benefits of the RbF-PDT for the CIGSe devices are widely described in the literature and mainly correlated with an increased open-circuit voltage (V_{OC}) [5, 8-10] and an improved fill factor (*FF*) [8-10]. However, in some cases in the contrary, a reduced *FF* was observed [11-13]. Such an inconsistency between the increase of V_{OC} and *FF* may suggest that the *FF* is reduced by negative effects on the series/shunt resistances or due to the formation of an extraction-barrier. As the reason for a higher V_{OC} and the improvement of the diode quality, a modification of the energy band alignment at the interface between CIGSe and CdS has been proposed [5, 8]. Specifically, RbF-PDT has been observed to lead to an additional downward band bending in the CIGSe absorber and a flat conduction band alignment upon interface formation with the CdS buffer [8]. This is in

agreement with a further reduced interface recombination observed by two different groups [14, 15], and could explain the increased lifetime described by Karki et al. [11]. The mechanism responsible for the band bending in the CIGSe as a result of RbF-PDT is yet under discussion. Karki et al. found a modification of the CIGSe surface by secondary ion mass spectroscopy measurements in the first 40 nm after RbF-PDT, with an increase in both Cu and In near the surface [11]. Taguchi et al. described their CIGSe films by a 50–100 nm thick Cu-deficient surface layer with a clear Ga depletion near the CIGSe/CdS interface [16]. It is this strong Cu depletion that might lead to a higher hole barrier at the grain boundaries and thereby to their improved passivation and finally to an increase in V_{OC} [9]. The discrepancy regarding the surface modification of the CIGSe can be ascribed to the different deposition procedures of the CIGSe absorbers that might induce differences in the surface composition. Partly responsible for the band alignment at the CIGSe-buffer interface might also be the formation of a secondary phase as a result of the RbF-PDT [17]. By means of transmission electron microscopy and X-ray photoelectron spectroscopy (XPS) analyses [16, 18], it was shown that an $RbInSe_2$ compound is formed in the CIGSe matrix. The segregation of such secondary phases at the CIGSe surface then results in a patterned surface morphology [8, 12, 16]. The extent to which the $RbInSe_2$ secondary phase is beneficial for the resulting device is not yet clear, however, Kodalle et al. [7] as well as Weiss et al. [13] suggest that this $RbInSe_2$ creates a current barrier at the hetero-interface. The severity of this barrier can be tuned either via the amount of incorporated Rb during the RbF-PDT [13] or via the thickness of an intentionally co-evaporated $RbInSe_2$ phase on CIGSe [7]. In particular, Kodalle et al. demonstrated that the *FF*-effect is dependent on the nominal composition of the bulk CIGSe, and only beneficial for a [Cu]/([In]+[Ga]) (*CGI*) ratio higher than 0.9 [7]. In other words, the formation of the secondary phases as a result of the RbF-PDT can be tuned by the PDT process as well as by the as-deposited characteristics of the CIGSe thin film.

To shed more light on the influence of the RbF on the CIGSe surface and in particular the formation of the $RbInSe_2$, we investigate the impact of a RbF-PDT on the surface of CIGSe absorbers intentionally prepared with different bulk composition in terms of the Cu content. Surface- as well as bulk- sensitive methods are used to examine an overall depth profile of the CIGSe composition, and a diffusion model is proposed explaining the effect of the RbF-PDT on the surface of the CIGSe absorber layer and the performance of the corresponding solar cells.

2. EXPERIMENTAL

Polycrystalline CIGSe thin films were prepared on 2 mm float glass (SGG Planiclear) covered with 800 nm thick Mo dc-sputtered single layer. The polycrystalline absorber layer was formed using a modified three-stage co-evaporation process, which is described in more detail in [19].

During the deposition of the CIGSe, its composition was controlled by optical real-time methods, i.e. laser light scattering and infrared light reflectometry. The Cu-concentration of the absorber layers is controlled by adjusting the duration of the third deposition stage. After reaching the second point of stoichiometry at the end of the second deposition stage, further co-evaporation of

In, Ga, and Se reduces the Cu-content of the CIGSe to CGI<1. For the experiment described here, two series of CIGSe samples were grown with CGI ratios of about 0.8 and 0.95 respectively. In both cases, a [Ga]/([In]+[Ga]) ratio (GGI) of approximately 0.35 was used. The bulk composition was confirmed by energy-dispersive X-ray spectroscopy. These CGI values were chosen to illustrate the best working absorbers in our lab (*CGI*=0.95) [7] in comparison to absorbers with a much reduced Cu content (*CGI*=0.8). For convenience, we will call these series "0.8CGI" (*CGI*=0.8) and "0.9CGI" (*CGI*=0.95). For each composition, two depositions were performed - one with and one without a RbF-PDT. The RbF-PDT was performed in situ in the same evaporation chamber as the CIGSe deposition for 10 min at a substrate temperature of 280 °C in the presence of Se. More details on the procedure of the PDT are discussed elsewhere [17]. Right after completing the absorber deposition, one SLG/Mo/CIGSe sample from each deposition run was stored in N_2 atmosphere minimizing the impact of air exposure. Furthermore, two Rb-containing samples of each series underwent an etching step in diluted aqueous ammonia (NH_3) solution (5 at. %) for 5 minutes at room temperature before they were stored in N_2 as well. This etching aims to mimic the chemical cleaning process that is performed before (and during) the deposition of the CdS buffer for completing CIGSe solar cells. Finally, all these samples were cut into small pieces of 4 mm x 8 mm in size and mounted on sample holders. One CIGSe, RbF-treated CIGSe and etched RbF-treated CIGSe sample of the "0.8CGI" and "0.95CGI" series each was then transferred to a hard X-ray photoelectron spectroscopy (HAXPES) analysis system. Finally, the same samples were analyzed by glow discharge optical emission spectroscopy (GD-OES) and scanning electron microscopy (SEM).

Additionally, one 5x5 cm² piece of each deposition run was used to fabricate complete solar cells in order to be able to connect the results of the measurements mentioned above with the performance of corresponding devices. The cells were finished by deposition onto CIGSe absorber of an approximately 50 nm thick CdS buffer layer prepared by chemical bath deposition as well as a i-ZnO/AZO double layer rf-sputtered with nominal thicknesses 40/110 nm respectively. A 2 µm thick Ni/Al/Ni front grid was deposited by electron beam evaporation on top of the complete solar cells to ensure good contacting conditions.

The HAXPES measurements were carried out at the BESSY II synchrotron in Berlin, Germany, namely at the HIKE end station operated at BESSY's KMC-1 beamline [20] during top-up mode of the storage ring with 298 mA ring current. At HIKE, an R4000 hemispherical photoelectron spectrometer manufactured by Scienta Gammadata optimized for high kinetic energies was used. For the experiments presented in this work, HAXPES was measured using excitation energies of 2030, 3000, 4000, 5000, and 6000 eV. The X-ray beam was horizontally polarized and irradiated the sample in grazing incidence configuration with an angle of 3° towards the surface of the sample, leading to a spot size in the order of 0.1 mm x 1 mm. Thereby, the beam intensity was monitored in an N_2-filled ionization chamber and kept constant. The rather big spot size on the sample reduced the influence of surface roughness and heterogeneities of the film composition on the measurement results. The released photoelectrons were detected in the polarization plane

perpendicular to the beam. For all measurements presented in this work, the entrance slit of the electron analyzer was kept constant at 0.5 mm and the pass energy was set to 200 eV.

A reference salt of GaF_3 was ordered from Santa Cruz Biotechnology. Inc. and used for XPS measurements with an Al K_α lab source.

The GD-OES depth profiles were measured using a GDA650-system built by Spectruma Analytik GmbH in pulsed rf mode, to be able to sputter-ablate the semiconducting absorber layer and to avoid heat-induced damage of the glass substrate. The system uses an Ar-plasma for sputtering and a CCD-array to detect the photons emitted during the relaxation. For the rf mode, the system is equipped with a Grimm-type glow discharge source including an anode with an inner diameter of 2.5 mm and a non-conducting cathode plate with front end coupling. More details about the GD-OES measurement and the utilized calibration for CIGSe samples can be found elsewhere [21]. SEM images of the CIGSe surface were recorded using a Zeiss LEO Gemini 1530 microscope with an acceleration voltage of 5 keV, electron backscatter diffraction (EBSD) data were measured using a Zeiss UltraPlus SEM equipped with an Oxford Instruments NordlysNano EBSD camera (acquisition and evaluation software AZtec). For the EBSD data in this manuscript, grains were selected whose surfaces are close to parallel to the substrate, and therefore, in good approximation, the measured grain orientation is also that of the substrate. To evaluate the coverage of the CIGSe surfaces, the *ImageJ* [22] software package was used: first, the image background was evaluated and subtracted, and then a brightness threshold for particle extraction from the underlying absorber was set. The uncertainty in brightness caused a rather high relative uncertainty of 20%, but the share of the covered surface was the same for both Cu-rich and Cu-poor absorbers. The current density–voltage (*j*-*V*) measurements were performed under standard test conditions (AM 1.5 spectrum, 1000 W/m^2, 25 ^{o}C) using a WACOM A+ solar simulator.

3. RESULTS

Figure 1 shows SEM images of the RbF-treated surfaces of both types of samples. On the surface of the “0.8CGI” sample the distribution and the (few nm) size of RbF-containing particles is much more uniform when compared to the “0.95CGI” CIGSe, which is covered by islands of different size and density depending on the CIGSe facets. An image analysis of the CIGSe surface suggested a fraction of 25±5 % coverage by Rb-containing islands (similar for both the “0.8CGI” and “0.95CGI” absorbers) and the size of these islands varied from a few to several 100 nm².

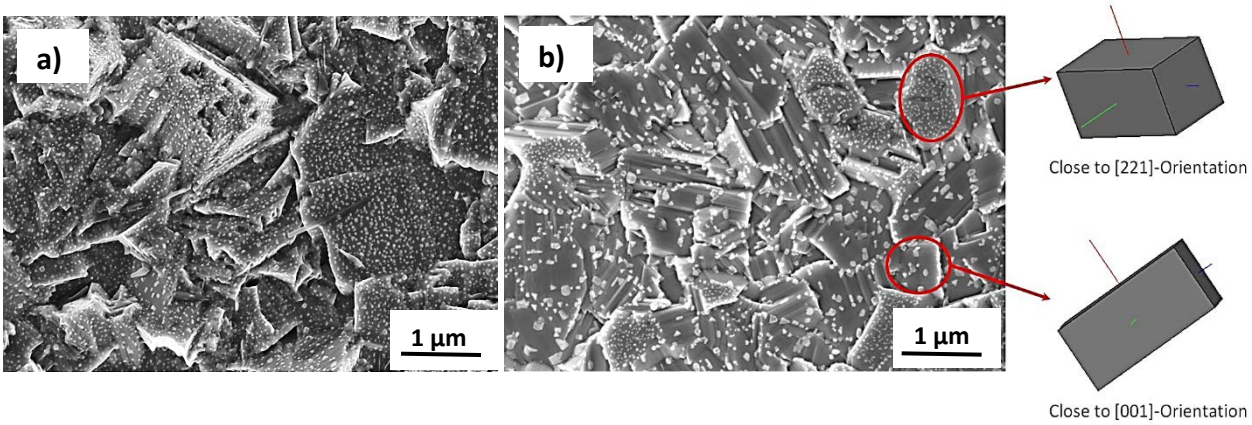

Figure 1. SEM images from the surface of RbF-covered CIGSe with (a) "0.8CGI" and (b) "0.95CGI" bulk compositions. On the right side of the figure, the orientation of the two CIGSe grains as measured by EBSD is indicated (in red circles), showing the dependence of the distribution of the Rb-containing phase on the orientation of the CIGSe.

An EBSD investigation of the surface of "0.95CGI" CIGSe demonstrates that this particle growth, initiated by the RbF-PDT, is denser, more uniform, and only a few nm small on grains with a [221] orientation, whereas on those with a [001] orientation, RbF particles are larger (several tens of nm in diameter) and not uniformly distributed. On the other hand, on the "0.8CGI" sample, the islands are completely homogeneously distributed, therefore, the distribution of RbF particles on the surface of the "0.8CGI" sample seems to not depend on the grain orientation of the CIGSe.

It was already reported by Witte et al. that the growth of the CdS buffer layer on top of PDT-free absorber layers is dependent on the orientation of the CIGS grains [23], while a more uniform coverage of the absorber layers by the CdS was found on samples with RbF-PDT [24, 25]. Similar to our results here, Witte et al. [23] found a dense and uniform coverage on [001]-oriented grains and a poor coverage on [221]-oriented grains. These authors explained this behavior with the lower surface energy of the [221]-oriented grains. We therefore assume a similar mechanism to influence the distribution of the RbF-particles (Figure 1). Additionally, an influence of the type of atoms at the very surface of the CIGSe and therefore the surface reconstruction on the distribution of the RbF seems possible. This, in turn, means that the surface energy and/or the reconstruction of the surface of the CIGSe-layer depend on the overall *CGI* of the CIGSe. It was already shown in literature that the Cu content and the density of Cu-related point defects, such as V_{Cu}, have an influence on the energies of the surfaces corresponding to grains with the [221]- and the [001]-orientations [26-28]. A corresponding influence of the *CGI* on the surface reconstruction will be discussed below.

It is interesting to note that not only the distribution and size of these islands but also the structure of the surface after etching the absorber with NH_3 is affected by the integral *CGI* of the CIGSe (see Figure S1 in the Supplementary Material). The "holes" remaining in the surface of the RbF-treated samples after NH_3-etching appear bigger and unevenly distributed in case of a Cu-rich

sample, while they are smaller and evenly distributed in case of a Cu-poor absorber layer. This behavior will also be discussed below.

3.1 Impact of the RbF-PDT on the performance of CIGSe solar cells

It is commonly known and therefore expected that the RbF-PDT has a positive impact on the performance of CIGSe-based solar cells [5-8]. This gain in efficiency is mainly attributable to an improved V_{OC} [5-7, 11-13]. In some studies, this increased V_{OC} is accompanied by an improved *FF* [5-7], just as one would expect [29], however, in other studies a reduced *FF* is shown despite the higher V_{OC} after alkali PDTs [7,11-13]. We recently proposed that this discrepancy is due to the interaction of Rb with point defects in the surface area of the CIGSe layer, whose concentration, in turn, depends on the composition of the CIGSe [7, 30]. Figures 2 and S2 exemplarily show that the RbF-PDT has a completely different effect on the device properties depending on the composition of the CIGSe absorber layer. Apart from a similar V_{OC}-boost for both RbF-treated CIGSe devices, the J_{SC} and mostly the *FF* are decreased considerably by the RbF-PDT in the case of the "0.8CGI" device. Here the detrimental effect on the *FF* comes along with dramatically affected series/shunt resistances (Figure 2e, 2f) by the RbF when the CIGSe absorber has the lower Cu concentration ("0.8CGI"). As a result, the RbF-PDT has reduced the efficiency of the "0.8CGI" device by ~2% absolute and increased the efficiency of the "0.95CGI" device by ~1% absolute (Figure 2d).

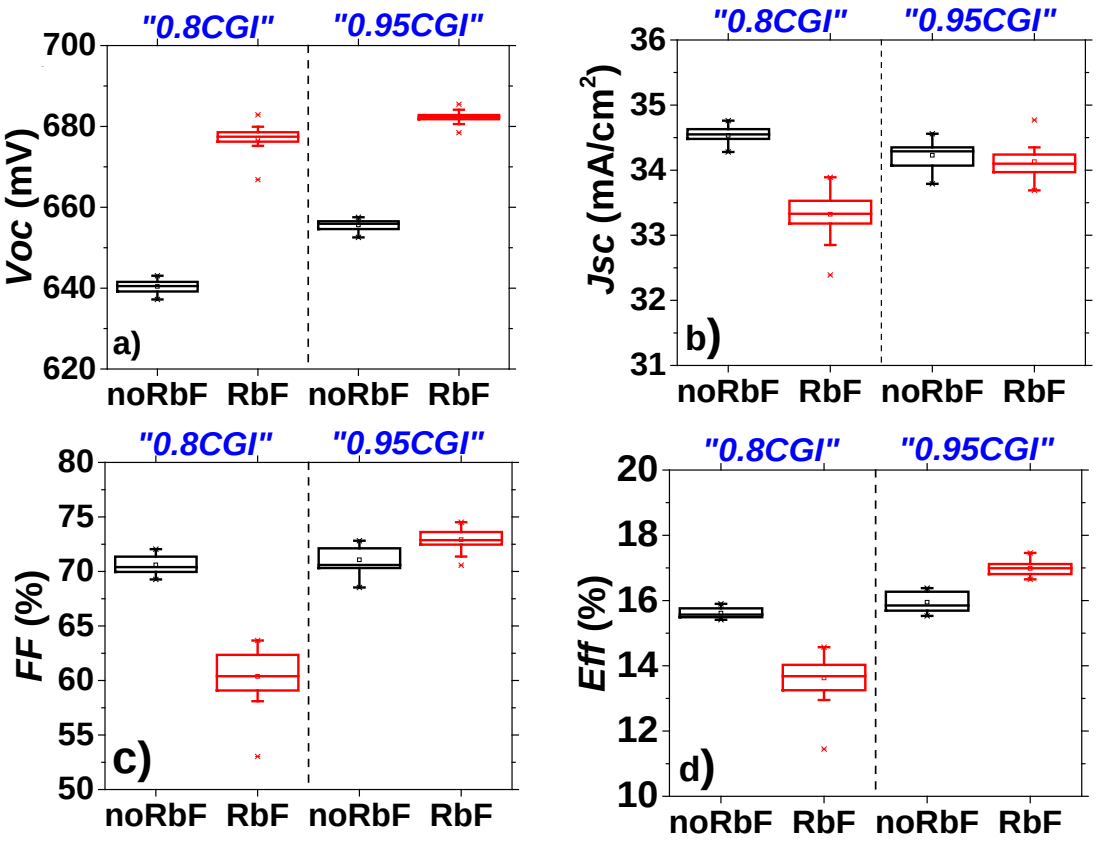

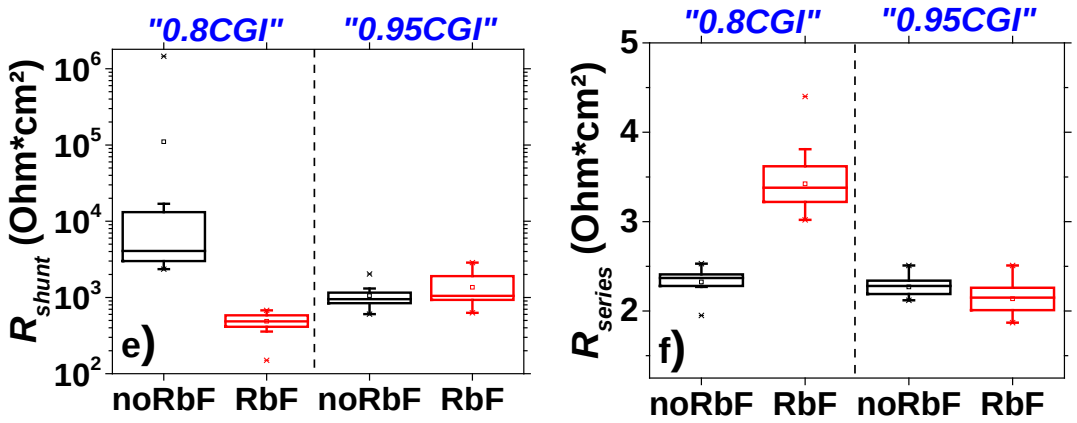

Figure 2. Boxplots of the PV-parameters of the solar cells based on "0.8CGI" and "0.95CGI" CIGSe absorbers before (*no RbF*) and after (*RbF*) the RbF-PDT (15 samples per box). Please note that this data has been shown previously in a separate study [7]. Furthermore, it could be shown that such "0.95CGI" absorber layers lead to efficiencies of up to 20.0 %, if the corresponding devices are prepared with an MgF_2 anti-reflective coating and a more sophisticated cell-separation [30].

In our previous study [7], we ascribed the *FF*-loss to a $RbInSe_2$ secondary phase forming during the RbF-PDT and acting as a current barrier at the interface between CIGSe and the CdS buffer. The thickness of this $RbInSe_2$ barrier was shown to depend on both Rb availability [12, 13] and the nominal composition of the CIGSe [7]. The fact that the formation of the $RbInSe_2$ layer can be suppressed (leading to a *FF*-recovery) only on absorber layers grown with a very close-to-stoichiometry composition [7] suggests that the RbF-PDT induces distinct surface modifications in CIGSe absorbers with different nominal composition. In the following sections we investigate in more detail the modifications of the surface morphology and composition during the RbF-PDT of the "0.8CGI" and "0.95CGI" absorber layers as well as modifications of the underlying bulk of the CIGSe.

3.2 Quantitative analysis of the CIGSe surface

Detailed HAXPES-spectra of the Cu $2p_{3/2}$, Ga $2p_{3/2}$, In $3d_{5/2}$, Se $2p_{3/2}$, Rb $3p_{3/2}$, Na 1s, and F 1s core levels were recorded for all six samples: bare CIGSe (CIGSe), RbF-treated CIGSe (CIGSe+RbF), and etched RbF-treated CIGSe (CIGSe+RbF+NH_3) for both the "0.8CGI" and "0.95CGI" series. To gain energy-dependent information of the elemental concentration ratios, the kinetic energy (E_{kin}) of the photoelectrons was varied by recording the spectra at five different photon energies in the range of $h\nu$ = 2–6 k*e*V. These excitation energies correspond to a range of information depths (*ID*) from ~4 nm to ~23 nm, calculated using the equation $ID = 3 \cdot \lambda_{CIGSe}$, where λ_{CIGSe} is the corresponding inelastic mean free path for an element in the CIGSe material (calculated using the TPP-2M formula [31]). For the determination of the line intensities of each

core level peak, the binding energies of the spectra were calibrated to that of Cu $2p_{3/2}$ (at 932.2 eV) and then integrated after a linear background was subtracted. All intensities were then normalized to the excitation intensity I_0, the inelastic mean free path λ_{CIGSe}, the transmission function of the analyzer T (provided by Gammadata Scienta) and the partial subshell photoionization cross-sections σ [32]. In the following, the normalized intensity is termed $I^{\Psi_{n,l}}$ for the respective core level $\Psi_{n,l}$. For the accuracy of this normalization we take into account the accuracy of 3% for the I_0 given by the signal deviation during the measurement, the 10% accuracy provided by Gammadata Scienta for T, the computational accuracy of 1% for σ [32], and the accuracy of 10% for λ_{CIGSe} [31].

The energy-dependent distribution of the CIGSe elements, as well as sodium, fluorine, and rubidium (normalized to the total concentration I^{tot}), is plotted in Figure 3 for the "0.8CGI" and "0.95CGI" samples. The error bars calculated by Gaussian error propagation reflect the determination accuracy of the normalized line intensities of each core level peak, whereas the dashed lines between the data points are only for guiding the eye. Sharp drops or increases in normalized intensity (for example, Se at 5 k*e*V in Figure 3a) will be disregarded here. We cannot explain nor relate them to a tendency, therefore, we can only conclude that such outlying data points result from unreproducible singular events that occurred during data acquisition at the synchrotron.

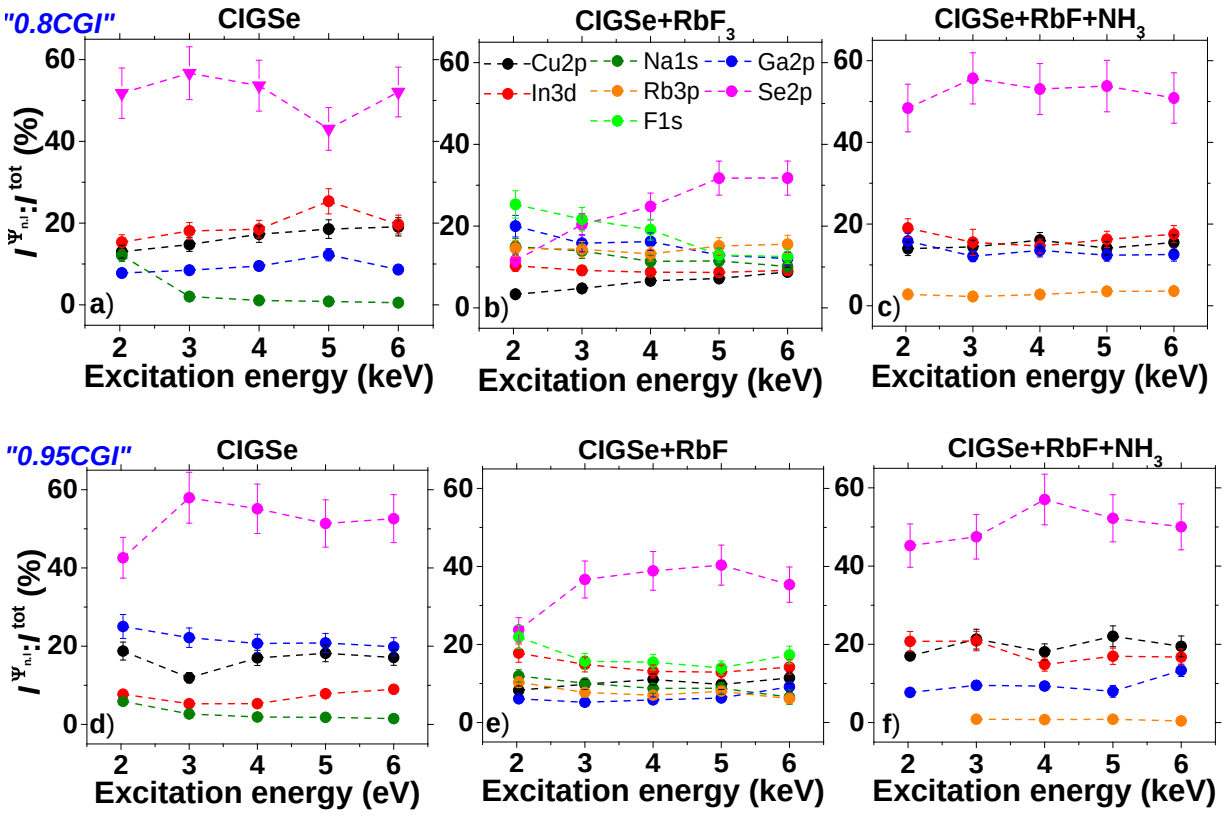

Figure 3. Energy-dependent distribution of the CIGSe composition in “0.8CGI” (a, b, c) and “0.95CGI” (d, e, f) samples before and after the RbF-PDT. The y-axis shows the ratio of the respective elemental signal to the sum of all signals. The legend in b) applies to all panels.

In the as-deposited absorbers (Figure 3a, 3d), all CIGSe elements are – within the errors of the measurements - uniformly distributed with an anticipated “more Cu-depleted” and “less Cu-depleted” surface for the “0.8CGI” and “0.95CGI” sample, respectively. A distinguishing feature of the as-deposited CIGSe samples is the inverted In/Ga prevalence from an In-rich to a Ga-rich surface composition induced by the increased Cu concentration from Cu-poor to Cu-rich CIGSe. The relatively high Ga-content in the latter sample might be connected to the co-evaporation process of CIGSe in the third stage, where we are just past the second stoichiometry point and In-Ga-Se diffuses into the sample. These conditions can lead to a Ga-enriched surface, an effect well described by Rodriguez-Alvarez [33]. In addition to these limiting conditions in a “0.95CGI” CIGSe layer (the regime where the layer is still rather close to a stoichiometric composition), there are very few available copper vacancies (V_{Cu}) as diffusion supporting sites, and hence, the *GGI* is locally high in a very thin surface layer. Another diffusion that we register for both as-deposited CIGSe samples is that of Na from the underlying glass towards the surface (stimulated by the absorber deposition, which is executed at elevated temperatures and possibly enhanced by the short air/humidity exposure of the absorber prior to its HAXPES characterization [19]).

The RbF-PDT denoted by the presence of Rb and F atoms (Figure 3b, 3e) seems to drive the surface copper into the bulk CIGSe, leaving a very Cu-depleted surface. Part of this decreased relative concentration of Cu might be due to the formation of additional Rb-containing islands on top of the CIGSe, which attenuate the Cu 2p signal more than that of the In 3d (at higher kinetic energy, therefore less attenuated). However, we have estimated that Rb-containing islands (Figure 1), covering ~25% of the surface, attenuate the CIGSe signals to a much lesser extent (Figure S3), supporting the effect of RbF on the Cu depletion. In contrast to copper, diffusion from the bulk to the surface of the CIGSe during the PDT is observed for Ga, Na, and to some extent for In. This effect appears to be more pronounced in the case of the “0.8CGI” sample, most probably due to a larger amount of available Cu vacancies. An opposite inversion of the In/Ga ratio is observed as a result of the RbF-PDT, i.e. from an In-rich to a Ga-rich composition in the case of the “0.8CGI” sample and from a Ga-rich to an In-rich composition for the “0.95CGI” sample. The changes in the I^{Se2p}/I^{tot} further reflect the difference in the diffusion of elements towards the surface: the closer to stoichiometry the composition of the absorber is, the less pronounced is the Se-depletion towards its surface after the RbF-PDT. Although such an apparent Se-depletion could also be caused by the attenuation of the Se_{2p} signal by a covering layer, we attribute the observed result to an actual diffusion process. As we already mentioned, the employed RbF-PDT covers only ~25% of the CIGSe surface (Figure 1) and only partially attenuates the Se 2p signal, not enough to explain the observed results (Figure S3). Another source of attenuation can be contamination of the air transferred samples, e.g. by a film of water formed on the CIGSe. However, a similar contamination is expected for all the investigated samples, since they were handled equally.

Therefore, we believe that in addition to the weak attenuations from RbF and the contamination layer, the predominant reasons for the changes in the Se 2p intensity are the diffusion processes at the very surface of the absorber.

To sum up, the dependence of the elements' concentration as a function of excitation energy for untreated and treated CIGSe samples suggests that there are three main effects of the RbF-PDT: (1) it enhances the Cu-depletion, especially in the near-surface region, (2) it affects the In/Ga prevalence, and (3) it promotes the diffusion of Na, Ga, and In towards the very surface.

After removal of the top RbF phase (together with most of the Na) by means of the NH_3 etch, a uniform distribution of most of the elements through the analyzed CIGSe surface is observed (Figure 3c, 3f). This means that when comparing the CIGSe and CIGSe+RbF+NH_3 samples, the net impact of the RbF-PDT on the surface composition of the CIGSe can be expressed as follows: (a) for the "0.8CGI" sample a slight decrease in Cu concentration and (to the same extent) an increase in the Ga concentration with a small In-enrichment at the near-surface, and (b) for the "0.95CGI" sample an inverted In/Ga prevalence from a Ga-rich to an In-rich surface.

3.3 Comparison between the surface and bulk composition

Figure 4 shows the ratios of the normalized intensities $I^{Cu2p}/(I^{In3d}+I^{Ga2p})$ (*CGI*) and $I^{Ga2p}/(I^{In3d}+I^{Ga2p})$ (*GGI*) as a function of photon energy for the two series of investigated samples. The so-called HAXPES thickness values are calculated as the average value between the minimum and maximum information depth *ID* of Cu $2p_{3/2}$, Ga $2p_{3/2}$, and In $3d_{5/2}$ into the CIGSe material [31]. As the HAXPES signal always contains information from the very surface to a depth well below the *ID*, this value does not correspond to a defined depth but more to an averaged depth information. This fairly coarse approximation, done for illustrative purpose only, allows us to show the cumulative - and energy dependent - composition from HAXPES analysis on the same graph with the thickness dependent *CGI* and *GGI* profiles from GD-OES measurements for the very same samples. The GD-OES profiles are aligned for comparability using the onset of the molybdenum signal [21]. Due to preferential-sputtering-induced artifacts of the GD-OES, the signal of the first few nm is adversely affected and often cannot be interpreted. Therefore, we removed the signal from the first ~50 nm of CIGSe and complemented the GD-OES results with HAXPES data. Such a combination of surface sensitive (HAXPES) and bulk sensitive (GD-OES) measurements on the same graph allows us to map the compositional changes from the very surface of the absorber into the depth of the thin film and finally towards the molybdenum back contact.

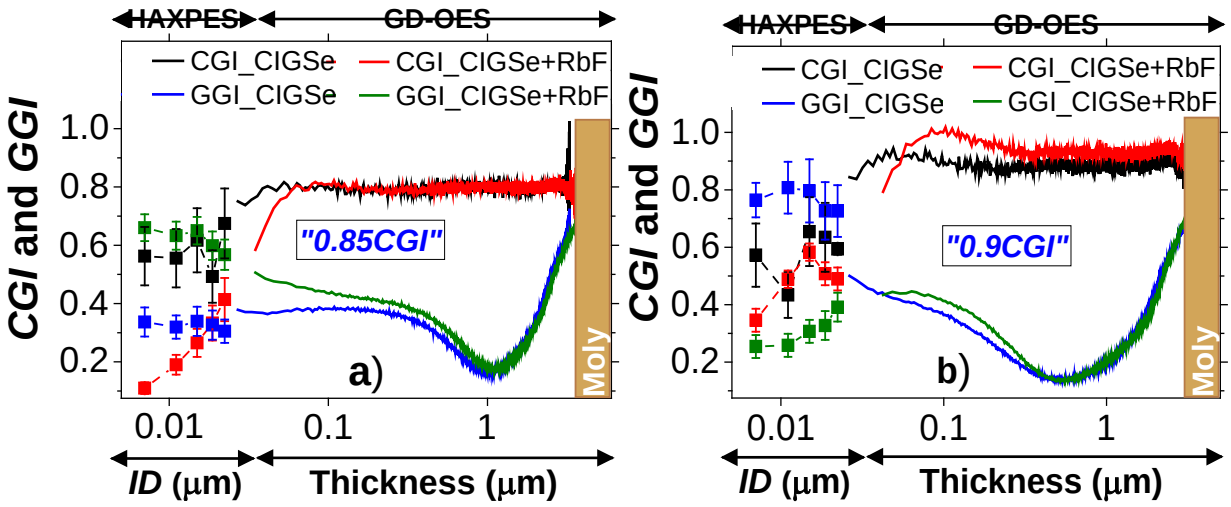

Figure 4. Surface (HAXPES) and bulk (GD-OES) distribution of the *CGI* and *GGI* versus the information depth *ID* and thickness, respectively, in CIGSe and CIGSe+RbF samples from "0.8CGI" (a) and "0.95CGI" (b) series. The combined plot on one x-axis was done for illustrative reasons only. The error bars indicated for HAXPES data were calculated by the Gaussian error propagation, whereas the relative standard deviation for the GD-OES measurements between 1.8% and 2.1% [21] has been discarded here to avoid an overloaded graph.

In the case of Rb-free "0.8CGI" CIGSe (Figure 4a), a steady *CGI* level of 0.8 (black line) is observed in the bulk of the absorber decreasing towards the surface down to a value of 0.7. HAXPES data show that at the very surface the *CGI* decreases even further, to slightly below 0.6. A similar reconstructed Cu-depleted surface was shown as a characteristic of co-evaporated CIGSe with a sub-stoichiometric composition [34]. Another agreement between GD-OES and HAXPES data is observed for the *GGI* values of the bare CIGSe (blue line): after the notch at about 1 μm depth from the surface, the *GGI* plateau of 0.35 is maintained up to the very surface.

When this "0.8CGI" CIGSe undergoes a RbF-PDT, only the very surface is affected. Both HAXPES and GD-OES measurements indicate that in comparison to the bare CIGSe, the *CGI* level (red line) drops earlier and steeper until it reaches a value of 0.1 (Figure 4a). On the *GGI* side, the RbF-PDT has the opposite effect (green line): after the minimum value of the notch, the *GGI* of the CIGSe+RbF sample is slightly higher in the bulk and gradually increases towards the surface where *GGI*≈0.6, which is almost twice as high as in the bulk of the CIGSe. This seems to be an effect of the previously mentioned Ga diffusion as a result of RbF-PDT towards the surface of the "0.8CGI" CIGSe (Figure 3a, 3b). Possible reasons for this will be discussed below.

In the case of "0.95CGI" CIGSe (Figure 4b), the *CGI* and *GGI* ratios behave differently. While the drop in the *CGI* from bulk to the surface for both CIGSe and CIGSe+RbF is comparable to the one in the "0.8CGI" case, the RbF-PDT raises the *CGI* value in the bulk of "0.95CGI" CIGSe. Moreover, the *GGI* profiles are dramatically different at the surface. From ~100 nm depth towards the very surface of the "0.95CGI" CIGSe, the *GGI* value jumps from ~0.4 to ~0.8 for the bare

absorber, but contrarily drops from ~0.45 to ~0.25 for CIGSe+RbF. In both cases, the transition from the bulk-sensitive GD-OES profiles to the HAXPES-data shows good agreement.

For the bare "0.95CGI" CIGSe, both *CGI* and *GGI* behaviors reflect the high concentration of Ga on the surface (Figure 3d). For the CIGSe+RbF, however, we again see the inversion of the In/Ga prevalence that was already observed from the distribution of CIGSe elements as a function of the excitation energy (Figure 3d, 3e) and is confirmed by the GD-OES profiles, which continue the *GGI* trends from the HAXPES analysis. Therefore, Figure 4 suggests that the *GGI* ratio at the very surface of the absorber can be dramatically increased either by the increase in Cu content or by the RbF-PDT, whereas a combination of the two approaches may result in a reduced *GGI* at the CIGSe surface. The effect of RbF on the surface composition, however, is almost reversible, since after the NH_3 etch the level of the surface *CGI* is recovered to reach 0.6 and 0.4, whereas the *GGI* changes to 0.25 and 0.45 for "0.95CGI" and "0.8CGI" CIGSe absorbers (Figure S4), respectively. Therefore, the final composition after RbF-PDT and etching of the surface is Cu-poorer, but Ga-richer in the case of the "0.8CGI" sample, as compared to the "0.95CGI" sample.

A conspicuous difference in the GD-OES spectra in case of the "0.95CGI" sample is that the *CGI* level in the bulk of CIGSe+RbF is not following the level of the bare CIGSe and almost reaches the stoichiometric composition at 0.1 μm thickness. This discrepancy might be an effect of high roughness of the CIGSe, which is changing from sample to sample but could also be an effect of different RbF coverage for "0.8CGI" and "0.95CGI" CIGSe (Figure 1).

3.4 Qualitative analysis of the CIGSe surface

Complementary to the quantitative investigation presented above, a qualitative analysis of the chemical shifts induced by the RbF-PDT and the subsequent etching was performed similar to studies presented earlier [12, 18]. Here, however, we qualitatively discuss HAXPES spectra measured at an excitation energy of 3000 eV instead of spectra taken with a lab-based XPS system. This energy was chosen in order to maintain a high surface sensitivity while reducing an influence from the surface oxides that are widely reported for air-exposed CIGSe absorbers [35-37]. The evolution of the surface composition for the "0.8CGI" CIGSe, CIGSe+RbF, and CIGSe+RbF+NH_3 samples is presented in Figure S5, whereas the respective spectra of the "0.95CGI" sample are shown in Figure S6 in the Supplementary Material.

Similar to the literature [12, 18], we find the respective chalcopyrite bonds in the core level spectra of the Rb-free samples [36], as well as an additional contribution to the Ga $2p_{3/2}$ spectrum, which belongs to a Ga-oxide. The latter can be seen exemplarily by the Auger spectrum of Ga $L_3M_{45}M_{45}$ (Ga LMM) of the "0.8CGI" sample with the Ga-II emission at $E_{kin} \approx 1062$ eV (Figure 5a), which indicates Ga_2O_3 – the first oxide to form on the CIGSe surface [36].

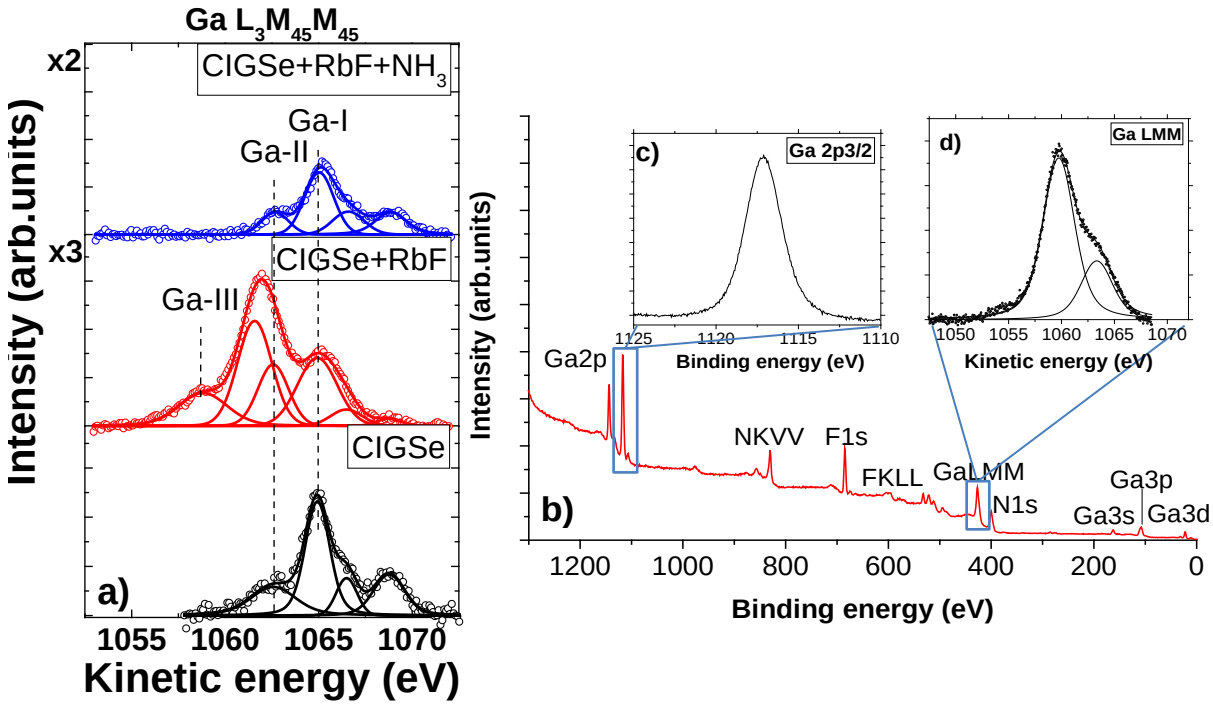

Figure 5. a) Ga LMM Auger spectra of the "0.8CGI" CIGSe samples measured at 3000 eV from as-deposited CIGSe (black), CIGSe+RbF (red), and CIGSe+RbF+NH_3 (blue); b) Survey spectrum with enlarged core-level spectrum of Ga2$p_{3/2}$ (c) and Auger spectrum of Ga LMM (d) measured with an Al K_α source from the reference GaF_3 salt.

As a result of the RbF-PDT, also In and Se oxides form at the surface (Figs. S5, S6, S7). In addition to the direct influence of the deposited RbF [12], this oxidation and hydroxylation of the surface of the RbF-treated CIGSe is promoted by the Rb-Na exchange mechanism [37, 38]. Moreover, the In-Se-O may also contain Rb (Figure 3) - residues of the RbF-PDT after the NH_3 etch that was demonstrated to be part of an $RbInSe_2$ secondary phase on the CIGSe surface [14, 15]. This corroborates our former findings [16]: due to the RbF-PDT, the surface of the CIGSe is covered by an Rb-In-(Se,O) secondary phase, which is incompletely removed by the NH_3 etch.

Another interesting effect of the RbF-PDT is the appearance of an additional Ga-contribution in the spectra of the Ga 2$p_{3/2}$ core level (Ga-3 in Figs. S5 and S6) and the spectra of the Ga LMM Auger emission (Ga-III in Figs. 5a and S8), respectively. Analyzing the emissions from the CIGSe+RbF sample and comparing them to those described in the literature, we can state that the binding energy (E_{bin}) of 1119.5 eV (Figure S5) and the Ga-III at $E_{kin} \approx 1059$ eV (Figure 5a) of the new Ga-3 contribution are smaller than the values reported for Ga_2O_3 [35, 36]. Barriere et al. demonstrated that at an energetic difference of more than 1 eV compared to Ga_2O_3 can be found for the Ga-F bond from the GaF_3 salt [39]. Moreover, we calculated the Auger parameters for the three features of the Auger and core level emissions (Table 1) and compared them to that of GaF_3 reference salt analyzed with a laboratory Al K_α source (Figure 5b-d) in our laboratory [40]. Based

on this analysis, we can confirm that the Ga-3 feature in the Ga $2p_{3/2}$ spectrum and Ga-III in the Ga LMM spectrum belong to the GaF_3 phase.

For the first time we detected this secondary phase *in vacuo* [16] on the surface of "0.95CGI" CIGSe (Figure S8) and now confirmed that it appears on a CIGSe surface independent of the CIGSe bulk composition (Figure 5a). A similar GaF_3 secondary phase was reported by Lepetit et al. to be formed on the surface of CIGSe after a KF-PDT [41].

Table 1. Modified Auger parameters (α') of CIGSe+RbF and GaF_3 salt.

Sample	**E_{kin} (Ga LMM), eV**		**E_{bin}(Ga2$p_{3/2}$), eV**		**α', eV**
CIGSe+RbF	Ga-I	1065.1 ± 0.2	Ga-1	1117.8 ± 0.1	2182.9 ± 0.3
	Ga-II	1062.0 ± 0.2	Ga-2	1118.5 ± 0.1	2180.5 ± 0.3
	Ga-III	1058.7 ± 0.2	Ga-3	1119.5 ± 0.1	2178.1 ± 0.3
GaF_3 salt		1059.7 ± 0.2		1117.1 ± 0.1	2176.8 ± 0.3

The RbF-PDT seems to be a driving force for the Ga diffusion towards the CIGSe surface - much stronger for the "0.8CGI" sample (Figure 3) and less noticeable for the "0.95CGI" that results in a larger or a smaller amount of GaF_3 on the absorber surface, respectively. This also means that after we remove the GaF_3 secondary phase during the ammonia wash (Figs. S5 and S6) the remaining surface will be Ga-rich, especially in the case of the "0.8CGI" sample.

DISCUSSION

By using the schematic representation of the two sample-sets in Figure 6 we discuss how the different nominal *CGI*s determine the lateral distribution of the layer stack and its in-depth evolution.

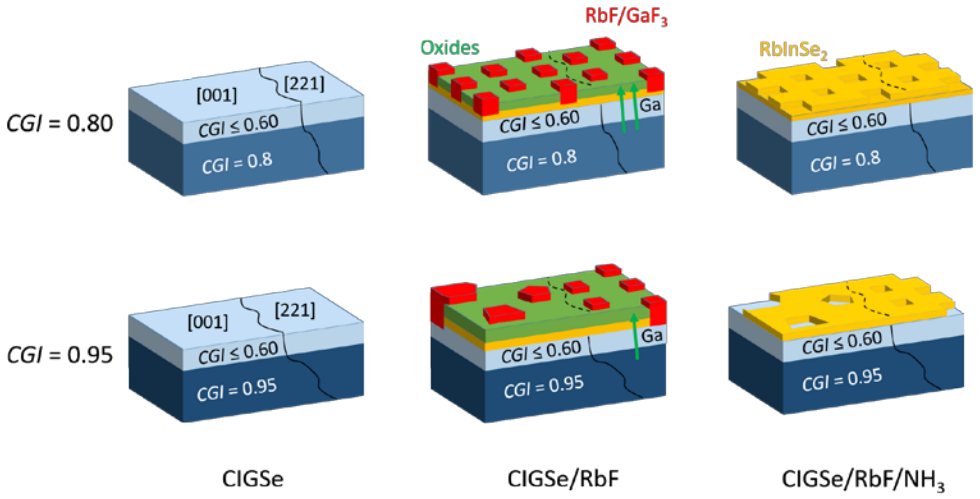

Figure 6. Schematic (not to scale) representation of the diffusion processes and phase formation at the surface of the CIGSe (left column), CIGSe+RbF (middle column), and CIGSe+RbF+NH_3 (right column) samples of the “0.8CGI” (top row) and “0.95CGI” (bottom row) sample sets. Please note that the "Oxides" layer refers to compounds that were formed from hydroxides and carboxides in addition to metal oxides.

For both series of CIGSe absorbers we register a characteristic Cu-depleted surface (with a *CGI*<0.6), underneath which the composition of CIGSe gradually changes within the first ~100 nm until the nominal *CGI* value is reached (Figure 4). However, after the RbF-PDT, HAXPES-data shows that the reduction of *CGI* on the surface depends on the nominal CIGSe composition and is stronger in the case of “0.8CGI” CIGSe (Figure S4) where a higher amount of V_{Cu} is expected. The same RbF-PDT covers the Cu-deficient surface of the CIGSe with islands of RbF-containing particles (Figure 1), whose density and distribution depend on the bulk composition of the CIGSe. On the “0.8CGI” CIGSe (Fig. 6 upper row) only a-few-nm wide RbF-containing islands are homogeneously distributed, whereas on the “0.95CGI” sample (Fig. 6, lower row) their growth is determined by the orientation of the CIGSe grains: denser, more uniform, and only a-few-nm large islands form on grains with [221] orientation, and larger (several 10 nm wide) and not uniformly distributed islands on the grains with [001] orientation (Figure 1). The remaining “holes” in the very surface of the NH_3-etched absorber layer show a similar dependence on the *CGI* (Figure S1), which helps to interpret their origin.

We have spectroscopically proven that this “Swiss-cheese like” surface contains Rb atoms that are bound to Se atoms exactly as in the $RbInSe_2$ reference [16]. Moreover, this secondary phase formed by the RbF-PDT is resistant to the ammonia etch and the amount of remaining $RbInSe_2$ on the CIGSe surface depends on the composition of the underlying absorber. In the case of the “0.95CGI” CIGSe, due to the limited amount of V_{Cu}, only little Rb incorporates into the absorber layer and only a thin, incompletely covering Rb- containing film forms (Figure 6). The F-compounds from the PDT and the O-compounds formed during the air transfer of the CIGSe form partly on the Rb-containing regions and partly on the CIGSe-layer, consequently depending on the

orientation of the CIGSe grains. In case of the "0.8CGI" sample, a thicker, denser $RbInSe_2$ film forms due to the abundantly available V_{Cu} at the surface and in the bulk of the CIGSe. Here, the F- and O-compounds grow directly on top of this layer; their density and distribution being independent of the grain orientation of the CIGSe. This effect might be additionally enhanced by the Rb- and Na-induced oxidation of the surface of the CIGSe. It was shown before that the oxidation of the surface can increase the surface energy of the CIGSe and therefore lead to a more uniform growth of subsequently deposited layers [23]. These surface modifications induced by the RbF-PDT, in turn, seem to be the reason for the improved coverage of the buffer layer on RbF-treated absorber layers [24, 25].

A thick $RbInSe_2$ barrier was shown to deteriorate the device performance [7] and it also explains the ~10% drop in the *FF* for our CIGSe device based on the "0.8CGI" absorber with RbF-PDT (Figure 3c). In the case of the "0.95CGI" device, the $RbInSe_2$ barrier appears to be thin/de-wetted enough to reduce the blocking of the diode current and thus to benefit from an improved bulk quality resulting in a higher *FF* [7, 13]. Consequently, as a result of the RbF-PDT, both the *FF* and the efficiency of our device based on the "0.95CGI" CIGSe absorber are increased from ~71% to ~73% and from ~16% to ~17%, respectively (Figure 2c, 2d).

Another side effect of the RbF-PDT is the formation of a GaF_3 secondary phase at the CIGSe surface (Fig.5, Table 1). Since GaF_3 can be formed by fluorides reacting with Ga_2O_3 [39] we assume that the above mentioned Rb- and Na-induced oxidation of the surface plays again a crucial role. The RbF-PDT acts as a driving force for Ga diffusion from the bulk of the absorber towards its surface (Figure 3). The amount of fluoride is larger on a "0.8CGI" surface, where we see more incorporated Rb and less pronounced in the "0.95CGI" case. This translates into a stronger diffusion of Ga towards the surface of the "0.8CGI" CIGSe absorber and therefore a higher Ga content at the surface after the removal of GaF_3 by the ammonia etch. The *GGI* values of ~0.45 and ~0.25 at the surface of "0.8CGI" and "0.95CGI" samples, respectively, confirm this (Fig. S4). We repeatedly found a similar Ga accumulation at the surface of absorbers with a *CGI* of 0.8 as a result of RbF-PDT in different experiments in our laboratory at PVcomB. Variations of *GGI* have been proved to directly affect the CIGSe band gap [43] and a *GGI* value of 0.3 is considered ideal at the CIGSe surface as it ensures a favorable flat conduction band alignment at the buffer interface [44]. An increase in *GGI* from 0.3 to 0.45 would widen the CIGSe's band gap from 1.15 eV to 1.3 eV and this will result in a change only in the conduction band offset of -0.15 eV [43]. According to Sozzi et al., such a change in the conduction band offset can additionally decrease the *FF* [45] as well as J_{sc} because a too steep front grading was theoretically proven to act as a barrier to prevent the minority carrier from diffusing into the buffer layer [46].

To sum up, in the case of devices based on Cu-poor CIGSe the performance is drastically damaged by the RbF-PDT because it creates a barrier for the diffusion of the minority carriers into the CdS buffer due to an overly thick $RbInSe_2$ film, and likely also due to a Ga accumulation at the CIGSe surface.

5. CONCLUSIONS

The effect of a RbF-PDT on the CIGSe absorber was investigated by a combination of surface elemental analysis (HAXPES) and bulk elemental analysis (GD-OES) with overlapping information depths. The changes in the CIGSe surface properties as a result of RbF demonstrate the key role of the absorber composition during the PDT. Due to the off-stoichiometric composition of both “0.8CGI” and “0.95CGI” CIGSe absorber layers (*CGI*=0.8 and *CGI*=0.95, respectively), their surface is reconstructed to form a strongly Cu-poor phase. Below this Cu-depleted surface, the composition of the CIGSe is gradually changing until ~100 nm of depth, where it reaches the bulk composition as seen in the GD-OES measurements. As a result of the RbF-PDT, the more Cu-poor the CIGSe composition is, the more GaF_3 and $RbInSe_2$ secondary phases form. Although GaF_3 is easily removed by the ammonia etch, the surface oriented Ga diffusion as a result of the RbF-PDT leaves behind a Ga-rich surface, which will form the interface with the CdS buffer layer. And again, the more Cu-poor the CIGSe surface is, the more Ga-rich surface will be left after the RbF-PDT. Such a Ga accumulation at the absorber-buffer interface changes the conduction band offset by ~0.15 eV and reduces the *FF* and J_{sc} of the device. On the other side, the remaining $RbInSe_2$ after the etch acts also as a current barrier at the same interface between the “0.8CGI” CIGSe and the CdS buffer leading again to a drop in the *FF*. By a change in the nominal *CGI* from 0.8 to 0.95 we decreased the detrimental effect of RbF-PDT on the CIGSe-based device on the account of thinning the $RbInSe_2$ secondary phase and avoiding the Ga accumulation at the CIGSe surface, improving the *FF* of the corresponding devices by ~12% absolute and their efficiency by ~3% absolute.

ACKNOWLEDGMENTS

The authors acknowledge financial support by the German Federal Ministry for Economic Affairs and Energy in the frame of the speedCIGS project (contract number 0334095E). H.A. Yetkin gratefully acknowledges the financial support of the Ministry of National Education of the Republic of Turkey. We also thank Helmholtz Zentrum Berlin for the allocation of synchrotron radiation beam time (172-05557-ST/R) and Dr. R. Félix for support during the measurements. For the preparation of the substrates we thank B. Bunn and K. Mayer-Stillrich, and for technical support we thank J. Lauche and T. Münchenberg.

ASSOCIATED CONTENT

Supplementary Material available: SEM images from the surface of RbF-covered CIGSe after the NH_3 etch (Figure S1); *j-V* curves for the solar cells based on “0.8CGI” and “0.95CGI” absorbers (Figure S2); Simulations of the attenuation effect from a RbF phase on CIGSe surface (Figure S3); Distribution of HAXPES CGI and GGI values for Cu-rich and Cu-poor CIGSe absorbers (Figure S4); Core-levels from both “0.8CGI” (Figure S5) and “0.95CGI” (Figure S6)

CIGSe; O1s and Na1s core level spectra from “0.8CGI” CIGSe (Figure S7); Ga LMM Auger spectra from “0.95CGI” CIGSe (Figure S8).

REFERENCES

[1] J.D. Major, M. Al Turkestani, L. Bowen, M. Brossard, C. Li, P. Lagoudakis, S.J. Pennycook, L.J. Phillips, R.E. Treharne, K. Durose, In-depth analysis of chloride treatments for thin-film CdTe solar cells, Nat Commun 7 (2016) 13231. https://doi.org/10.1038/ncomms13231

[2] N. Spalatu, J. Hiie, R. Kaupmees, O. Volobujeva, J. Krustok, I. Oja Acik, M. Krunks, Postdeposition processing of SnS thin films and solar cells: prospective strategy to obtain large, sintered, and doped SnS grains by recrystallization in the presence of a metal halide flux, ACS Appl. Mater. Interfaces 11 (2019) 17539–17554. https://doi.org/10.1021/acsami.9b03213

[3] P. Jackson, D. Hariskos, E. Lotter, S. Paetel, R. Wuerz, R. Menner, W. Wischmann, M. Powalla, New world record efficiency for Cu(In,Ga)Se_2 thin-film solar cells beyond 20%, Prog. Photovolt: Res. Appl. 19 (2011) 894–897. https://doi.org/10.1002/pip.1078

[4] A. Chirilă, P. Reinhard, F. Pianezzi, P. Bloesch, A.R. Uhl, C. Fella, L. Kranz, D. Keller, C. Gretener, H. Hagendorfer, D. Jaeger, R. Erni, S. Nishiwaki, S. Buecheler, A.N. Tiwari, Potassium-induced surface modification of Cu(In,Ga)Se_2 thin films for high-efficiency solar cells, Nat. Mater. 12 (2013) 1107−1111. https://doi.org/10.1038/nmat3789

[5] P. Jackson, R. Wuerz, D. Hariskos, E. Lotter, W. Witte, M. Powalla, Effects of heavy alkali elements in Cu(In,Ga)Se_2 solar cells with efficiencies up to 22.6%, Phys. Status Solidi RRL 10(8) (2016) 583−586. https://doi.org/10.1002/pssr.201600199

[6] M. Nakamura, K. Yamaguchi, Y. Kimoto, Y. Yasaki, T. Kato, H. Sugimo, Cd-free Cu(In,Ga)(Se,S)$_2$ thin-film solar cell with record efficiency of 23.35%, IEEE J. Photovolt. 9(6) (2019) 1863−1867. https://doi:10.1109/JPHOTOV.2019.2937218

[7] T. Kodalle, T. Bertram, R. Schlatmann, C.A. Kaufmann, Effectiveness of a RbF post deposition treatment of CIGS solar cells in dependence on the Cu-content of the absorber layer, IEEE J. Photovolt., 9(6) (2019) 1839−1845. https://doi:10.1109/JPHOTOV.2019.2929418

[8] S. Ishizuka, N. Taguchi, J. Nishinaga, Y. Kamikawa, S. Tanaka, H. Shibita, Group III elemental composition dependence of RbF post deposition treatment effects on Cu(In,Ga)Se_2 thin films and solar cells, J. Phys. Chem. C 122(7) (2018) 3809−3817. https://doi.org/10.1021/acs.jpcc.8b00079

[9] R. Wuerz, W. Hempel, P. Jackson, Diffusion of Rb in polycrystalline Cu(In,Ga)Se_2 layers and effect of Rb on solar cell parameters of Cu(In,Ga)Se_2 thin-film solar cells, J. Appl. Phys. 124 (2018), 165305. https://doi.org/10.1063/1.5044629

[10] E. Avancini, R. Carron, T.P. Weiss, C. Andres, M. Bürki, R. Figi, Y.E. Romanyuk, S. Buecheler, A.N. Tiwari, Effects of rubidium fluoride and potassium fluoride postdeposition treatments on Cu(In,Ga)Se_2 thin films and solar cell performance, Chem. Mater. 29 (2017) 9695−9704. https://doi.org/10.1021/acs.chemmater.7b03412

[11] D. Hauschild, D. Kreikemeyer-Lorenzo, P. Jackson, T. Magorian Friedlmeier, D. Hariskos, F. Reinert, M. Powalla, C. Heske, L. Weinhardt, Impact of a RbF postdeposition treatment on the electronic structure of the CdS/Cu(In,Ga)Se_2 heterojunction in high-efficiency thin-film solar cells, ACS Energy Lett. 2 (2017) 2383−2387. https://doi.org/10.1021/acsenergylett.7b00720

[12] D. M. Heinemann, T. Kodalle, C. Hages, M. Klupsch, D. Greiner, L. Korte, S. Levcenco, T. Unold, R. Schlatmann, C.A. Kaufmann, Evaluation of recombination losses in thin film solar cells using an LED sun simulator - the effect of RbF post-deposition on CIGS solar cells, EPJ Photovoltaics 9 (2018) 9. https://doi.org/10.1051/epjpv/2018006

[13] S. Karki, P. Paul, G. Rajan, B. Belfore, D. Poudel, A. Rockett, E. Danilov, F. Castellano, A. Arehart, S. Marsillac, Analysis of recombination mechanisms in Rbf-treated CIGS solar cells, IEEE J. Photovolt. 9 (2019) 313–318. https://doi:10.1109/JPHOTOV.2018.2877596

[14] N. Taguchi, S. Tanaka, S. Ishizuka, Direct insights into $RbInSe_2$ formation at Cu(In,Ga)Se_2 thin film surface with RbF postdeposition treatment, Appl. Phys. Lett. 113 (2018) 113903. https://doi.org/10.1063/1.5044244

[15] M. Malitckaya, H.-P. Komsa, V. Havu, M.J. Puska, Effect of alkali metal atom doping on the $CuInSe_2$-based solar cell absorber, J. Phys. Chem. C 121 (2017) 15516–15528. https://doi.org/10.1021/acs.jpcc.7b03083

[16] N. Maticiuc, T. Kodalle, J. Lauche, R. Wenisch, T. Bertram, C.A. Kaufmann, I. Lauermann, In vacuo XPS investigation of Cu(In,Ga)Se_2 surface after RbF postdeposition treatment, Thin Solid Films 665 (2018) 143–147. https://doi.org/10.1016/j.tsf.2018.09.026

[17] T. Kodalle, D. Greiner, H.A. Yetkin, M. Klupsch, C. Li, P.A. van Aken, I. Lauermann, R. Schlatmann, C.A. Kaufmann, Elucidating the mechanism of a RbF post deposition treatment in CIGS thin film solar cells, Sol. RRL 2(9) (2018) 1800156. https://doi.org/10.1002/solr.201800156

[18] T.P. Weiss, S. Nishiwaki, B. Bissig, R. Carron, E. Avancini, J. Löckinger, S. Buecheler, A.N. Tiwari, Injection current barrier formation for RbF postdeposition-treated Cu(In,Ga)Se_2-

based solar cells, Adv. Mater. Interfaces 5 (2018) 1701007. https://doi.org/10.1002/admi.201701007

[19] M.D. Heinemann, R. Mainz, F. Österle, H. Rodriguez-Alvarez, D. Greiner, C.A. Kaufmann, T. Unold, Evolution of opto-electronic properties during film formation of complex semiconductors, Sci. Rep. 7 (2017) 48463. https://doi.org/10.1038/srep45463

[20] M. Gorgoi, S. Svensson, F. Schäfers, G. Öhrwall, M. Mertin, P. Bressler, O. Karis, H. Siegbahn, A. Sandell, H. Rensmo, W. Doherty, C. Jung, W. Braun, W. Eberhardt, The high kinetic energy photoelectron spectroscopy facility at BESSY progress and first results, Nuclear Instruments and Methods in Physics Research Section A: Accelerators, Spectrometers, Detectors and Associated Equipment 601 (2009) 48–53. https://doi.org/10.1016/j.nima.2008.12.244

[21] T. Kodalle, D. Greiner, V. Brackmann, K. Prietzel, A. Scheu, T. Bertram, P. Reyes-Figueroa, T. Unold, D. Abou-Ras, R. Schlatmann, C.A. Kaufmann, V. Hoffmann, Glow discharge optical emission spectrometry for quantitative depth profiling of CIGSe thin-films, J. Anal. At. Spectrom. 34 (2019) 1233–1241. https://doi.org/10.1039/C9JA00075E

[22] C.A. Schneider, W.S. Rasband, K.W. Eliceiri, NIH Image to ImageJ: 25 years of image analysis, Nature Methods 9(7) (2012) 671–675. https://doi.org/10.1038/nmeth.2089

[23] W. Witte, D. Abou-Ras, D. Hariskos, Chemical bath deposition of Zn(O,S) and CdS buffer: influence of Cu(In,Ga)Se_2 grain orientation, Appl. Phys. Lett. 102 (2013) 051607. https://doi.org/10.1063/1.4788717

[24] T. Magorian Friedlmeier, P. Jackson, D. Kreikemeyer-Lorenzo, D. Hauschild, O. Kiowski, D: Hariskos, L. Weinhardt, C. Heske, M. Powalla, A closer look at initial CdS growth on high-efficiency Cu(In,Ga)Se_2 absorbers using surface-sensitive methods, Proceedings of the 43rd IEEE PVSC 2016, 457–461. https://doi:10.1109/PVSC.2016.7749634

[25] T. Kodalle, L. Choubrac, L. Arzel, R. Schlatmann, N. Barreau, C.A. Kaufmann, Effects of KF and RbF post deposition treatments on the growth of the CdS buffer layer on CIGS thin films - a comparative study, Sol. Energ. Mat. Sol. 200 (2019) 109997. https://doi.org/10.1016/j.solmat.2019.109997

[26] J.E. Jaffe, A. Zunger, Defect-induced nonpolar-to-polar transition at the surface of chalcopyrite semiconductors, Phys. Rev. B 64 (2001) 241304(R). https://doi.org/10.1103/PhysRevB.64.241304

[27] S.B. Zhang, S.-H. Wei, Reconstruction and energetics of the polar (112) and ($1^{-}1^{-}2^{-}$) versus the nonpolar (220) surfaces of $CuInSe_2$, Phys. Rev. B 65 (2002) 081402(R). https://doi.org/10.1103/PhysRevB.65.081402

[28] S. Siebentritt, N. Papathanasiou, J. Albert, M.Ch. Lux-Steiner, Stability of surfaces in the chalcopyrite system, Appl. Phys. Lett. 88 (2006) 151919. https://doi.org/10.1063/1.2192638

[29] M.A. Green, Solar Cell Fill Factors: General Graph and Empirical Expressions, Solid State Electron 24(8) (1981) 788–789.

[30] T. Kodalle, Unraveling the structural and optoelectronic effects of Rb on chalcopyrite solar cells. Doctoral Thesis, Martin-Luther-University, Halle-Wittenberg, Germany, 2020. http://dx.doi.org/10.25673/33525

[31] S. Tougaard, QUASES-IMFP-TPP2M program, Quases-Tougaard Inc., 2002.

[32] M.B. Trzhaskovskaya, V.I. Nefedov, V.G. Yarzhemsky, Photoelectron angular distribution parameters for elements z = 1 to z = 54 in the photoelectron energy range 100–5000 eV, At. Data Nucl. Data Tables 82 (2002) 257–311. https://doi.org/10.1006/adnd.2002.0886

[33] H. Rodriguez-Alvarez, R. Mainz, S. Sadewasser, A one-dimensional Fickian model to predict the Ga depth profiles in three-stage Cu(In,Ga)Se_2, J. Appl. Phys. 115 (2014) 204913. https://doi.org/10.1063/1.4880298

[34] H Mönig, Ch.-H. Fischer, R. Caballero, C.A. Kaufmann, N. Allsop, M. Gorgoi, R. Klenk, H.-W. Schock, S. Lehmann, M.Ch. Lux-Steiner, I. Lauermann, Surface Cu depletion of Cu(In,Ga)Se_2 films: An investigation by hard X-ray photoelectron spectroscopy, Acta Materialia 57 (2009) 3645–3651. https://doi.org/10.1016/j.actamat.2009.04.029

[35] R. Würz, M. Rusu, Th. Schedel-Niedrig, M.Ch. Lux-Steiner, H. Bluhm, M. Hävecker, E. Kleimenov, A. Knop-Gericke, R. Schlögl, In situ X-ray photoelectron spectroscopy study of the oxidation of $CuGaSe_2$, Surf. Sci. 580 (2005) 80–94. https://doi.org/10.1016/j.susc.2005.01.054

[36] J. Lehmann, S. Lehmann, I. Lauermann, T. Rissom, C.A. Kaufmann, M.Ch. Lux-Steiner, M. Bär, S. Sadewasser, Reliable wet-chemical cleaning of natively oxidized high-efficiency Cu(In,Ga)Se_2 thin-film solar cell absorbers, J. Appl. Phys. 116 (2014) 233502. https://doi.org/10.1063/1.4903976

[37] C. Heske, R. Fink, E. Umbach, W. Riedl, F. Karg, Na-Induced effects on the electronic structure and composition of Cu(In,Ga)Se_2 thin film surfaces, Appl. Phys. Lett. 68 (1996) 3431–3433. https://doi.org/10.1063/1.115783

[38] A. Vilalta-Clemente, M. Raghuwanshi, S. Duguay, C. Castro, E. Cadel, P. Pareige, P. Jackson, R. Wuerz, D. Hariskos, W. Witte, Rubidium distribution at atomic scale in high efficient Cu(In,Ga)Se_2 thin-film solar cells, Appl. Phys. Lett. 112(10) (2018) 103105. https://doi.org/10.1063/1.5020805

[39] A.S. Barriere, G. Coutier, G. Gevers, H. Gukgan, T. Seguelond, A. Thabti, Preparation and characterization of gallium (iii) fluoride thin films, Thin Solid Films 173 (1989) 243–252. https://doi.org/10.1016/0040-6090(89)90140-5

[40] I. Lauermann, M. Bär, C.H. Fischer, Synchrotron-based spectroscopy for the characterization of surfaces and interfaces in chalcopyrite thin-film solar cells, Sol. Energ. Mat. Sol. 95 (2011) 1495–1508. https://doi.org/10.1016/j.solmat.2010.12.042

[41] T. Lepetit, G. Ouvrard, N. Barreau, KF post deposition treatment in co-evaporated $Cu(In,Ga)Se_2$ thin film solar cells: beneficial or detrimental effect induced by the absorber characteristics, Prog. Photovolt: Res. Appl. 25 (2017) 1068–1076. https://doi.org/10.1002/pip.2924

[42] T. Kodalle, R. Kormath Madam Ragupathy, T. Bertram, N. Maticiuc, H.A. Yetkin, R. Gunder, R. Schlatmann, T.D. Kühne, C.A. Kaufmann, H. Mirhosseini, Properties of co-evaporated $RbInSe_2$ thin films, Phys. Status Solidi RRL 13 (2019) 1800564. https://doi.org/10.1002/pssr.201800564

[43] M. Turcu, I. M. Kötschau, U. Rau, Composition dependence of defect energies and band alignments in the $Cu(In_{1-x}Ga_x)(Se_{1-y}S_y)_2$ alloy system, J. Appl. Phys. 91 (2002) 1391–1399. https://doi.org/10.1063/1.1432126

[44] L. Weinhardt, O. Fuchs, D. Groß, G. Storch, E. Umbach, N. G. Dhere, A. A. Kadam, S. S. Kulkarni, C. Heske, Band alignment at the $CdS/Cu(In,Ga)S_2$ interface in thin-film solar cells, Appl. Phys. Lett. 86 (2005) 062109. https://doi.org/10.1063/1.1861958

[45] G. Sozzi, F. Troni, R. Menozzi, On the combined effects of window/buffer and buffer/absorber conduction-band offsets, buffer thickness and doping on thin-film solar cell performance, Sol. Energ. Mat. Sol. 21 (2014) 126–136. https://doi.org/10.1016/j.solmat.2013.10.037

[46] M. Topič, F. Smole, J. Furlan, Band-gap engineering in $CdS/Cu(In,Ga)Se_2$ solar cells, J. Appl. Phys. 79 (1996) 8537-8540. https://doi.org/10.1063/1.362533